Astron. Astrophys. 338, 132–138 (1998)

ASTRONOMY
AND
ASTROPHYSICS

Near-infrared adaptive optics imaging of dust shells around five late-type stars with COME-ON+⋆

P. Cruzalèbes[1], **B. Lopez**[2], **M. Bester**[3], **E. Gendron**[4], **and B. Sams**[5]

[1] Observatoire de la Côte d'Azur, Département Fresnel UMR 6528, Av. Copernic, F-06130 Grasse, France (cruzalebes@obs-azur.fr)
[2] Observatoire de la Côte d'Azur, Département Fresnel UMR 6528, BP 4229, F-06034 Nice Cedex 4, France (lopez@obs-nice.fr)
[3] Space Sciences Laboratory, University of California at Berkeley, Berkeley, CA 94720-7450, USA (manfred@ssl.berkeley.edu)
[4] Observatoire de Paris - Meudon, DESPA, F-92195 Meudon Cedex, France (egendron@hplyot.obspm.fr)
[5] Mediateam, Weidenweg 2c, D-85375 Neufahrn, Germany (sams@mediateam.de)

Received 15 January 1998 / Accepted 26 June 1998

Abstract. Near-infrared images of circumstellar dust shells around five late type stars have been obtained with the ESO - COME-ON+ adaptive optics system in 1994 September. Full angular resolution of the 3.60 m ESO - La Silla telescope was achieved at 1.25, 1.65 and 2.2 μm (respectively 0.09, 0.12 and 0.15 $''$ of angular resolution). A dynamic range of 1000:1 is obtained in the images.

Key words: circumstellar matter – stars: imaging – stars: late type – stars: AGB and post-AGB

1. Introduction

The study of the physical mechanisms by which stars, at each phase of their evolution, enrich the interstellar medium by losing their material is of high interest to stellar physics. All stars with initial mass on the main sequence between 1 to 8 $M_{\odot}$(solar masses) stay in the so-called Asymptotic Giant Branch (AGB) before producing a planetary nebula. This stage is characterized by an ejection of mass, continuous or violent, producing an extended circumstellar shell of dust and gas. Many questions concerning the physical mechanisms which drive the mass loss and the processes which govern the formation and the destruction of the dust grains have still no answer. A large number of observations suggest that the mass loss increases and deviates from spherical symmetry while the star evolves along the AGB. A preliminary survey has led to the result that at least half of the sources are non-spherical (Dougados 1991). A further mid-IR imaging and millimeter interferometric mapping study of more than 50 evolved stars (Meixner 1993) has also led to the conclusion that the last stage of AGB mass loss is inherently aspherical. In this context, we have proposed to obtain diffraction-limited images in the near infrared (J, H and K) of a small sample of well studied and well documented late type stars for which photometric, spectroscopic and polarimetric data are available. Our sample of objects consisted of both oxygen-rich and carbon-rich stars at various phases of their evolution and with various shell opacities. Some of them exhibit a non-spherical geometry shown by the polarization measurements, the observed bipolar structure and the difficulty to fit accurately the observed broad band spectrum with classical spherical models (Rown-Robinson & Harris 1983a, 1983b). The near-infrared domain helps to probe the hot dust component and the structure associated to the inner circumstellar envelope. The inner radius of the dust envelope is a particularly critical parameter in the dust formation modelling. The measurements obtained with the Infrared Spatial Interferometer (ISI) provide some constraints on the mass loss mechanisms (Danchi et al. 1994). Recent long baseline interferometric observations at 11 μm have shown, for example, that the supposed well-known Mira star o Ceti displays a geometrical asymmetry of its shell structure (Lopez et al. 1997a). The geometrical shell parameters, the dust density law, the extinction opacity and constraints on the dust grain sizes can be deduced (Lopez et al. 1995). Presently the dust shell morphology is best studied with imaging systems rather than with 2-telescope interferometry which just leads to one-dimensional visibility curves. Although the angular resolution of a 3.60-m telescope class does not allow to resolve the central star and the inner shell, the interest of adaptive optics lies in its capability of imaging the large scale structures.

2. Observations

The high angular resolution images presented in this paper have been obtained at the 3.60-m telescope of ESO-La Silla with the COME-ON+ adaptive optics system on 1994 September 21. The combination of the high angular resolution and the high sensitivity offered in the near infrared by this instrument was essential for the project (Rigaut et al. 1991). On one hand, the expected size of the region responsible for the near-infrared circumstellar emission needs the angular resolution allowed by the full correction (0.09 $''$ at J). On the other hand, the brightness ratio between the unresolved central star and the resolved circumstellar shell needs a high dynamic range (about 1000:1)

Send offprint requests to: P. Cruzalèbes

⋆ Based on observations collected at the European Southern Observatory, La Silla (Chile)

Table 1. Program stars

Object	RA (2000.0)			Dec (2000.0)			Sp. Type	m_V	m_I	m_J	m_H	m_K	m_L	m_M	$F_{12\mu}$	$\emptyset_K$
	(h)	(m)	(s)	(°)	(′)	(″)									(Jy)	(″)
CRL 618	06	19	58.2	-10	38	14	B8V	8.8		6.5	5.0	3.5	1.3	0.1	420	1
VY CMa	07	22	58.2	-25	46	03	M3I-II	7.8	4.9	2.0	0.5	-0.7	-2.9	-4.2	9920	0.1
TX Psc	23	46	23.5	03	29	14	C5,2-C7,2	5.1	1.8	0.9	-0.2	-0.6	-0.9	-0.9	160	0.2
α Sco	16	29	24.4	-26	25	54	M1.5Ib	1.0	-1.7	-2.7	-3.6	-3.9	-4.2	-3.9	3200	2
o Ceti	02	19	20.7	-02	58	28	M7IIIe	4.7	-0.9	-2.0	-2.3	-3.1	-3.7	-3.8	4888	0.1

allowed by the instrument. In order to increase the contrast in the resulting image without saturating the NICMOS array when observing the brightest stars ($m_K < 0$) of our sample, a large number of short exposure frames (0.1 to 3.0 s) have been co-added. The non-saturation of the array was ensured during the acquisition process. This has also been controlled a posteriori by measuring the maximum level of intensity of each frame.

The visible magnitudes of all our targets are also well in agreement with the sensitivity of the wavefront sensor which uses the central parts of our objects themselves as reference stars. Source calibrators (non-resolved stars) have also been observed in view of a posteriori deconvolution.

Fig. 1 is the long exposure map of the calibration star λ Psc. Three symmetrical parts of the first Airy ring can be seen near the center. The lowest contour is about 3 times the standard deviation of the noise and is equal to 0.1 % of the maximum of intensity (corresponding to a dynamic range of 1000:1). The noise has been measured in 10 by 10 pixel boxes situated at each corner of the long exposure image of the calibrator.

Table 1 (at the end of the paper) lists the program stars together with their spectral types, broad band magnitudes (V magnitudes are at the maximum of luminosity), and angular diameter of their inner dust shell, measured with the ISI interferometer (Danchi et al. 1994) or estimated (Rowan-Robinson & Harris 1983a, 1983b). The observations are summarized in Table 2 and were obtained during the night from 1994 September 21 to 22.

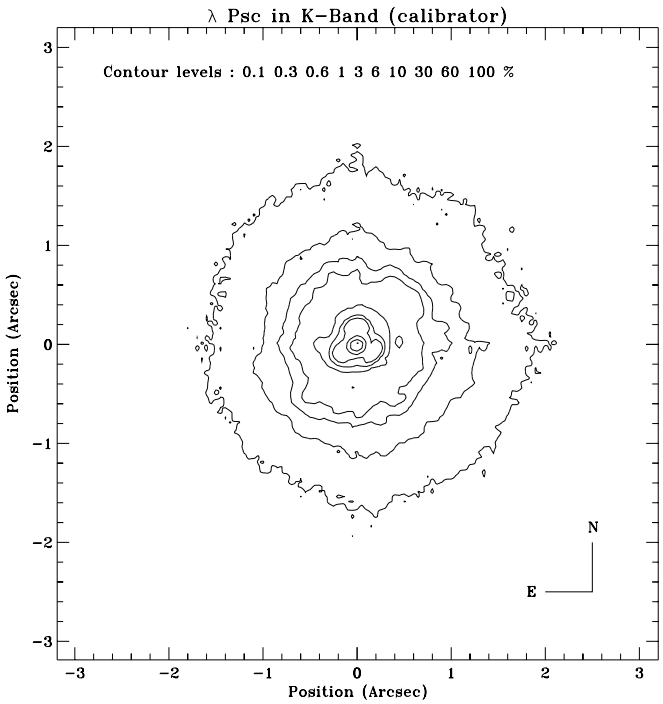

Fig. 1. Long exposure map of the calibration star λ PSC in K-band (total integration time of 1300 s). North is up and east is left. Overplotted contours are 0.1, 0.3, 0.6, 1, 3, 6, 10, 30, 60, and 100 % of the maximum of intensity. The lowest contour is three times the standard deviation of the noise, measured in 10 by 10 pixel boxes situated at the corners of the map.

3. Data analysis procedure

The observations were carried out using the MPE infrared high resolution camera, SHARP (Hofmann et al. 1993), at the 3.60-m telescope of the European Southern Observatory (ESO) at La Silla, Chile. SHARP uses a 256×256 pixel NICMOS 3 detector array developed by Rockwell International Corporation with the parameters summarized in Table 3. This array is split into four 128×128 quadrants, each of them having an independent data acquisition channel. A system of digital signal processors allows continuous read-out of the array as fast as 10 Hz, as well as on-line image processing for quick-look purpose. With an image scale of 0.05″ per pixel the camera is used for diffraction limited imaging at J (1.25 μm), H (1.65 μm) and K (2.2 μm) bands.

In order to eliminate instrumental effects (flat field, sky, dead pixels, ...), data cubes of hundreds of exposure frames have been stored with the observed object centered in two opposite quadrants from one data cube to the other.

The image processing was done using the MPE InfraRed Speckle Interferometry reduction software IRSI (Eckart & Duhoux 1990). Standard infrared data reduction software was applied to each individual frame : quadrant extraction, dead pixel removal, sky subtraction, flat fielding. Then, these frames have been co-added using the Shift-and-Add algorithm. The same processing has been applied both to the program targets and to the reference stars. Finally, a deconvolution process derived from the Lucy algorithm has been used to show the low level structures in the dust shells (Lucy 1974). The lowest contour of each reconstructed map has been limited to 0.1 % of the maximum of intensity, in agreement with the dynamic range of 1000:1 of the calibrators.

Table 2. Logbook of the observations

Target	λ_{CVF} (μm)	#frames	τ_{exp} (s)	T_{int} (s)
α Sco	2.2	1900	0.3	570
TX Psc	2.2	2800	0.3	840
λ Psc (ref)	2.2	1300	1.0	1300
o Ceti	1.25	1200	0.5	600
70 Ceti (ref)	1.25	1000	0.5	600
o Ceti	1.65	2800	0.5	1400
70 Ceti (ref)	1.65	2800	0.5	1400
o Ceti	2.2	1200	0.5	600
70 Ceti (ref)	2.2	400	3.0	1200
CRL 618	2.2	2000	1.0	2000
6 Mon (ref)	2.2	1500	1.0	1500
VY CMa	2.2	120	1.0	120
		280	0.5	140
HR 2786 (ref)	2.2	200	0.5	100

Table 3. Camera parameters (Böker et al. 1994)

Detector material	HgCdTe
Detector size	256×256 pixels
Pixel size	40×40 μm
Read noise in	
Read-reset-read mode	60 e^-
Peak quantum efficiency	0.6
Spectral response	0.8-2.5 μm
Operation temperature	77 K

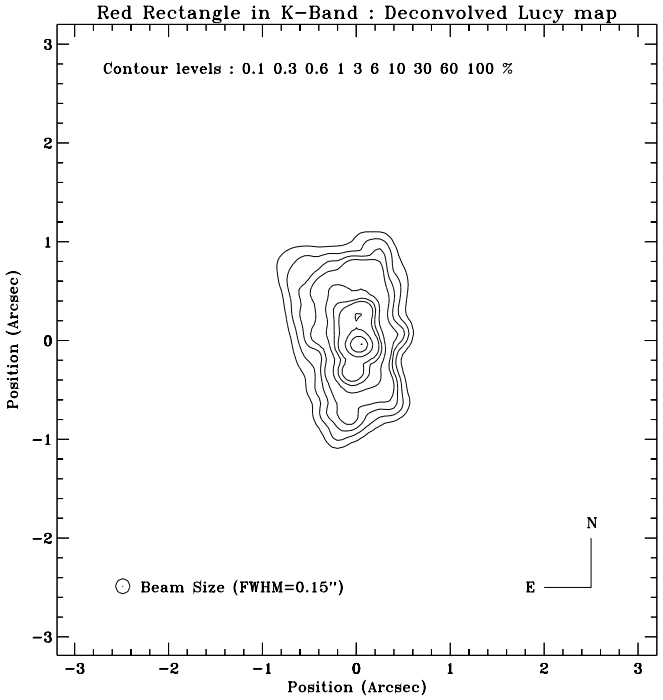

Fig. 2. Reconstructed Lucy map of the Red Rectangle nebula in K-band (total integration time of 2000 s). North is up and east is left. The angular resolution is 0.15 ″ . Overplotted contours are 0.1, 0.3, 0.6, 1, 3, 6, 10, 30, 60, and 100 % of the maximum of intensity.

The orientation of the maps on the sky is based on the well-known bipolar morphology of the Red Rectangle nebula. We have compared our 2.2 μm COME-ON+ reconstructed map of the Red Rectangle with an angular resolution of 0.15 ″ to the map we previously obtained by infrared speckle interferometry at the 3.60-m CFH Telescope with a comparable resolution in the same spectral band (Cruzalèbes et al. 1996). The overall shape, i.e. a North-South extension of the nebula with a position angle of about 15 ° to the east, is similar. The North-Eastern lobe is also dominant at this wavelength. Moreover, recent ESO-ADONIS observations that we carried out in 1997 January confirmed the right orientation of our previous COME-ON+ maps, mainly thanks to the confirmation of the presence of the North-Eastern clump of dust at a distance of 1.3 ″ of the central star of VY CMa (Monnier et al. 1998).

4. Discussion and results

4.1. The Red Rectangle

The Red Rectangle nebula (AFCRL 618-1343, AFGL 915) is a remarkable carbon-rich symmetrical nebulosity embedding the ninth V magnitude post-AGB star HD 44179. The photographic images in red light by give the object a rectangular shape of nearly 1 arcmin on the sky and show spikes marking an X-shape (Cohen et al. 1975). Many observations have been carried out at high angular resolution in the infrared. In 1993 December, adaptive optics images were obtained through narrow band filters centered on 1.647 μm (bandwith : 18 nm) and 0.850 μm (bandwidth : 75 nm) at the 3.60-m CFHT (Roddier et al. 1995). In 1991 May, J, H, K, L and M maps were obtained using the COME-ON+ experiment at the ESO 3.60-m (Rouan 1993). Speckle images were reconstructed from CFHT data (Hawaii) on 1990 December in L and M and from KPNO 3.80-m data (Kitt Peak) on 1987 November in K (Cruzalèbes et al. 1996). L images were also produced from the same CFHT speckle data set (Tessier et al. 1990). A tomographic reconstructed map was also produced at K (Leinert & Haas 1989). Earlier, the sizes of both the extended and the compact emissions were estimated from K, L and M observations (Dainty et al. 1985) and from H, K, L and M measurements (Dyck et al. 1984).

Fig. 2 shows our Lucy-deconvolved map of the Red Rectangle nebula, obtained at K (2.2 μm) with a total integration time of 2000 s. The envelope is clearly non spherical, roughly rectangular. The general orientation of the nebula is of 10 ° (from North to East). At a level of 0.1 % (related to the dynamic range of 1000:1), its dimensions are 2.2 × 1.4 ″. As previously seen in speckle maps (Cruzalèbes et al. 1996), the overall shape of the nebula is bipolar. The X shape is clearly visible, interpreted as light scattered by material distributed on the surface of a bicone (Roddier et al. 1995). The total angle of the cone is about 45 ° and its axis is aligned on the axis of the rectangular nebula (10 ° from North to East). The North-Eastern lobe is more extended

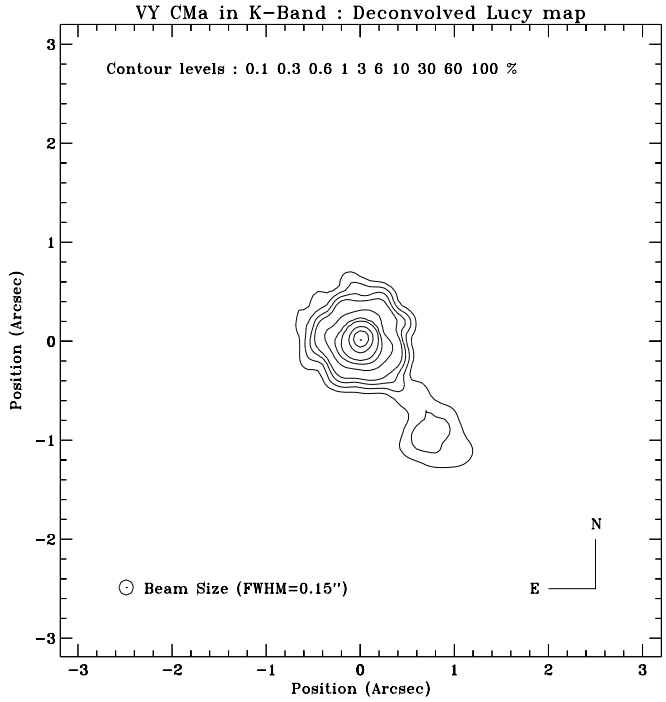

Fig. 3. Reconstructed Lucy map of VY CMa in K-band (260 s of total integration time). North is up and east is left. The angular resolution is 0.15 ″ . Overplotted contours are 0.1, 0.3, 0.6, 1, 3, 6, 10, 30, 60, and 100 % of the maximum of intensity.

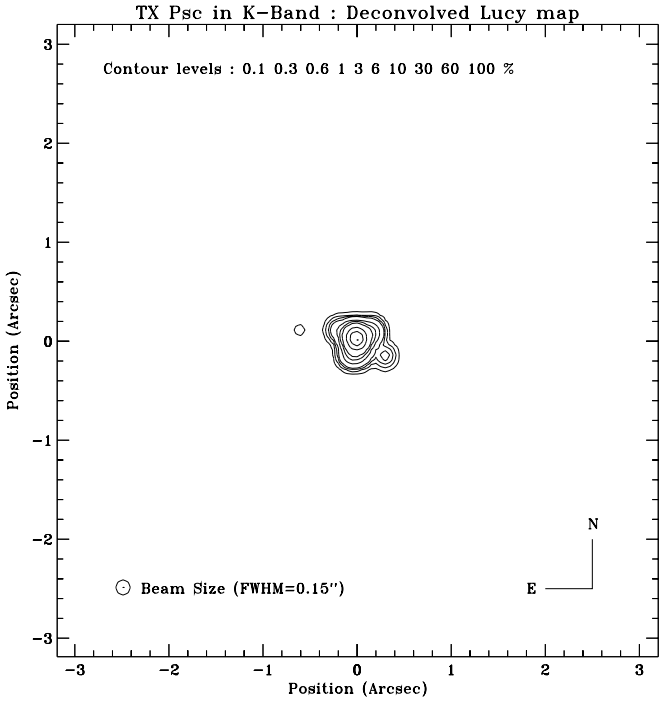

Fig. 4. Reconstructed Lucy map of TX Psc in K-band (840 s of total integration time). North is up and west is left. The angular resolution is 0.15 ″ . Overplotted contours are 0.1, 0.3, 0.6, 1, 3, 6, 10, 30, 60, and 100 % of the maximum of intensity.

than the South-Western one, as seen in the previous IR speckle maps (Cruzalebes et al. 1996). A secondary maximum is also present at a level of intensity of 20 %, at a distance of 0.3 ″ from the central maximum and at a position angle of 169 °. Recent radiative transfer modelling of the dust shell has explained the shape of the nebula and led to the extraction of some dust parameters as well as to an estimation of the mass of the dust shell of $3.8 \times 10^{-4}\ M_{\odot}$ (Lopez et al. 1997b).

4.2. VY Canis Majoris

The object VY CMa (M3I-II) is one of the strongest emitters in the infrared (Hyland et al. 1969). It has a reflection nebulous structure. Although it has been intensively observed with photometry, polarimetry, imagery and interferometry, it is still not clear today whether it is a very young star still in formation, in a pre-main-sequence stage of its evolution (Herbig 1970), or an evolved one, in a post-main-sequence star (Hyland et al. 1969). Observations carried out on 1981 January at the ESO 3.60-m telescope at La Silla from 1 to 5 μm have shown that VY CMa is resolved at all wavelengths and that its diameter decreases from 0.215 ″ at 1 μm to 0.136 ″ at 2.2 μm and then increases to 0.183 ″ at 4.8 μm (Bensammar et al. 1985).

Fig. 3 shows that the dust shell surrounding the central star is clearly resolved at K (with a total integration time of 260 s) and quasi spherical with a full width at 0.1 % of the maximum of about 1.4 ″ . It also shows a structure at a distance of about 1.3 ″ in the SW direction with a position angle of 216 °. This quasi-circular clump, never seen before, has a relative intensity level of 0.4 % and an angular diameter of about 0.9 ″ . It may be an accumulation of dust possibly accreted by a non visible companion star. This hypothesis needs further observations at other wavelenghts to be confirmed.

4.3. TX Piscium

The semi-regular variable of spectral type between C5,2 and C7,2 TX Piscium is one of the carbon stars best observed at HRA. Lunar Occultation events were recorded between 1992 and 1994 at wavelengths ranging from 0.55 to 3.6 μm (Richichi et al. 1995). The authors interpreted substantial departure from the simple photospheric model of circular disk as due to the presence of warm dust in an optically thin shell very close to the central star, possibly clumpy, and/or the presence of large star spots, areas of lower temperature or results of obscuration by intervening dust clumps very close to the star. Recent determination of the angular diameter has also been determined at 0.712 μm (12 nm of bandwidth) and at 0.8 μm (22 nm of bandwidth) at the Mark III Optical Interferometer from 1989 august to 1992 september, finding a diameter varying between 9.4 mas (millisecond of arc) and 11.1 mas (Quirrenbach et al. 1994). Clumps were also detected by CO mapping with the IRAM 30-m telescope in the (2-1) and (1-0) transitions, interpreted as evidence for erratic and non spherically symmetric outflow of matter in the envelope (Heske et al. 1989).

Fig. 4 shows the Lucy-reconstructed map of TX Piscium. The dust shell surrounding the central star is well resolved in K (840 s of total integration time), roughly circular with a diameter of about 0.7 ″ at a level of 0.1 % (related to the dynamic range of 1000:1). A clump, with a size smaller than 0.25 ″ and a level of intensity of about 2 %, is detected in the SW direction (position angle of 241 °) close to the central star at about 0.35 ″ of distance. This tends to confirm the clumpy interpretation of the Lunar Occultation data (Richichi et al. 1995), even if the clumps suggested by LO were supposed to be much closer to the central star (some milliseconds of arc).

4.4. α Scorpii

The M1.5 supergiant and visual binary Antares has a well known dust shell extending up to many stellar radii from the star. No significant amount of dust closer to 1 ″ was found from the visibility measurements at 11 μm with the ISI interferometer (Bester et al. 1996). At this wavelength, the authors have measured an angular diameter of 44.4 $\pm$ 2 mas (millisecond of arc). The angular diameter of the supergiant was determined with the ESO 3.60-m telescope by means of lunar occultation (Richichi & Lisi 1990). The authors claimed a good agreement between their photospheric angular diameter of 41.3 mas at 2.43 μm, and the later interferometric measurements at 0.6 μm (bandwidth of 55 nm) (Bedding et al. 1994). They suspected possible deviations from the simple model of a circular, homogeneous photospheric disk. The presence of non-centro-symmetric features was established from interferometric data, leading to a "disk + 1 spot" model (Tuthill 1994). In addition, observations at various wavelengths and with various techniques revealed that Antares and its blue companion star are surrounded by a shell composed of ionized gas and dust extending about 2.5 ″ in diameter (Bloemhof et al. 1984). Ionization calculations based on ultraviolet high resolution spectroscopic measurements led to the estimation of the inner radius of the expanding circumstellar envelope around the M-star of about 8.5 $R_\star$ (stellar radii) (van der Hucht et al. 1980).

Fig. 5 shows our diffraction-limited map of Antares in the K-band (570 s of total integration time). The circumstellar dust shell is roughly ovalized, elongated to the East (position angle of 44 °) and lies on about 0.9 $\times$ 0.5 ″ (at 0.1 % level). Many clumps are detected close to the star : one at a distance of 0.2 ″ with a position angle of 337 ° (barely separated from the central star); another at a distance of 0.3 ″ with a position angle of 217 °; and the last at a distance of 0.4 ″ (well resolved) with a position angle of 258 ° and a relative intensity of 2 %. This West-East extension is in apparent contradiction with the 10 μm images of IRTF, which found a North-South extended emission (Danchi et al. 1992). The origin of that misagreement is not clear, maybe instrumental (residual smearing of the 10 μm images from the chopper which had a North-South throw). Further high angular observations at higher dynamic range are needed to understand the various orientations of the extended emission.

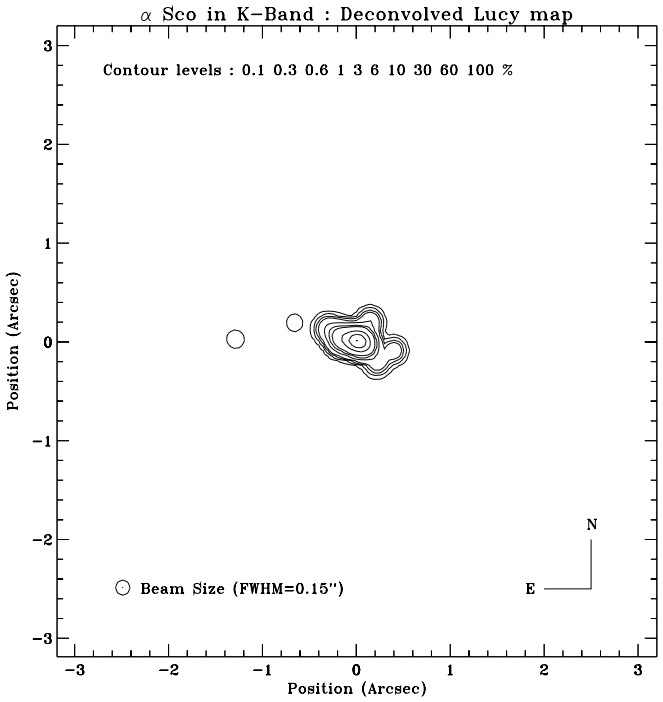

Fig. 5. Reconstructed Lucy map of a Sco in K-band (570 s of total integration time). North is up and east is left. The angular resolution is 0.15 ″ . Overplotted contours are 0.1, 0.3, 0.6, 1, 3, 6, 10, 30, 60, and 100 % of the maximum of intensity.

4.5. o Ceti

Although o Ceti belongs to the first targets of early speckle interferometry (Bonneau et al. 1982), departures from circular rotational symmetry were noted only recently. Many high angular resolution observations at optical wavelengths were interpreted in terms of an ellipticity of the photosphere (Karovska et al. 1991; Haniff et al. 1992; Wilson et al. 1992; Quirrenbach et al. 1992). A very recent modelling work, based on visibility observations at 11 μm with the ISI interferometer during the time period 1988-1995, proposed different non-spherical models to fit the interferometric data, one of which emphasizing inhomogeneities or clumps within the dust shell (Lopez et al. 1997a).

For this star only of our sample, we carried out multiple infrared wavelength imaging with COME-ON+. We obtained images in J at 1.25 μm (Fig. 6), H at 1.65 μm (Fig. 7) and K at 2.2 μm (Fig. 8) with respectively 600 s, 1400 s and 600 s of total integration time. In each infrared band, the dust shell is clearly resolved. Our observations confirm that the distribution of the circumstellar matter around o Ceti is asymmetrical.

The circumstellar dust shell in J measures about 1 ″ (at 0.1 % level). Two elongated and parallel low-level structures appear in J along an axis oriented at 321 ° north to east. The brightest one (that to the south) lies at a distance of about 1 ″ from the central star, has an extension of about 1.0 $\times$ 0.4 ″ with a level of intensity of 0.7 %. The faintest one (that to the north) lies at a distance of about 1.4 ″ from the central star, is separated from

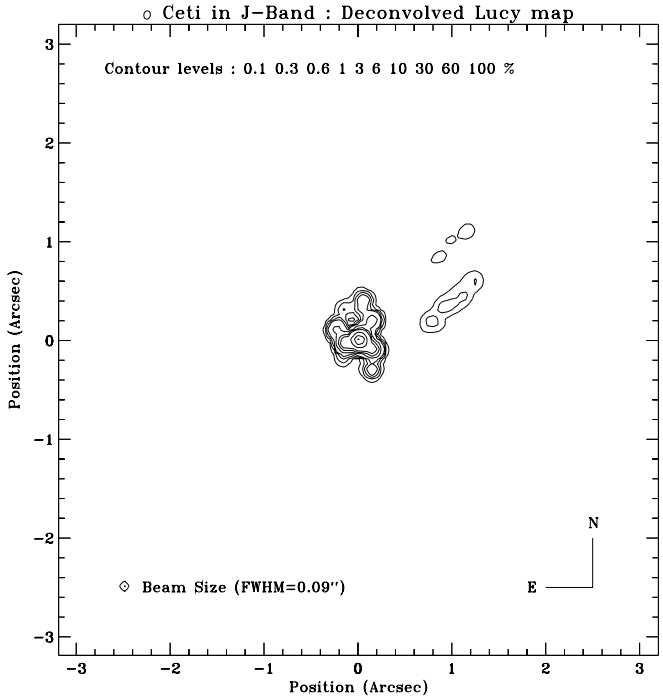

Fig. 6. Reconstructed Lucy map of o Ceti in J-band (600 s of total integration time). North is up and east is left. The angular resolution is 0.09″. Overplotted contours are 0.1, 0.3, 0.6, 1, 3, 6, 10, 30, 60, and 100 % of the maximum of intensity.

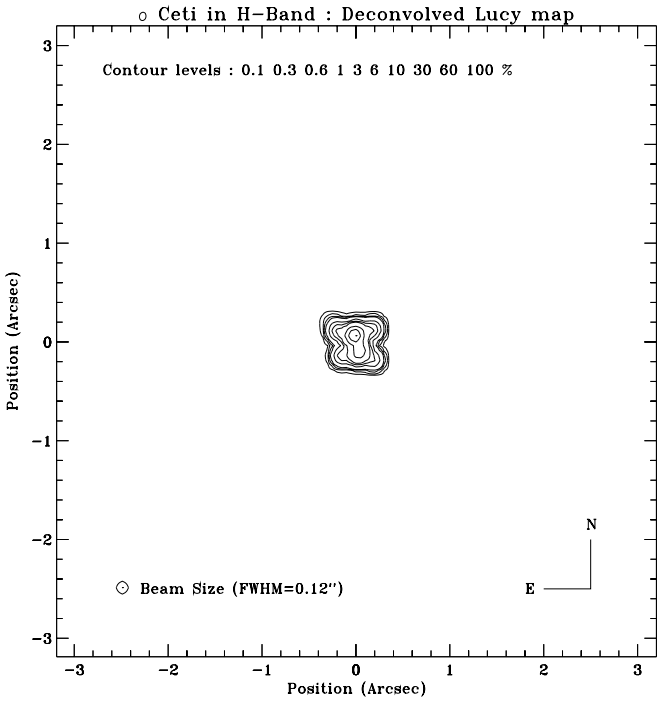

Fig. 7. Reconstructed Lucy map of o Ceti in H-band (1400s of total integration time). North is up and east is left. The angular resolution is 0.12″. Overplotted contours are 0.1, 0.3, 0.6, 1, 3, 6, 10, 30, 60, and 100% of the maximum of intensity

the southern structure by 0.6 ″ , has an extension at 0.1 % of about 0.8 × 0.3 ″ , and a maximum intensity of 0.3 %. These 2 elongated structures, never seen before, suggest that clumps of dust may be present there. These clumps are not in concordance with the position of the companion (a white dwarf surrounded by an accretion disk) : speckle observations of 1990 showed the companion at a distance of 0.61 ″and a position angle of 111 ° (Karovska et al. 1993).

The H map shows a quasi square dust shell, 0.8 ″at a level of 0.1 %, North-South oriented. A secondary maximum is seen very close to the central star, at a distance of 0.15 ″ (the angular resolution is 0.12 ″), at a position angle of 192 °, with an relative intensity of about 50 %. The shape of the shell can be seen as a small vertical X. The opening angle of its arms is about 93 °. One can notice that the upper-right arm (to the North-West) roughly follows the axis of the low level structures appearing in J (position angle of 314 ° for this arm).

The K map confirms the X shape of the shell, its orientation and its opening angle. In this spectral band, the shell is more extended, roughly 1.3 ″ at 0.1 % level. The upper-right arm is still in the direction of the J elongated structures (P.A. of 316 °). This X shape of the shell was never suspected before. Even the best maps previously published (Haniff et al. 1992) taken at 700.7, 709.9 and 650.0 nm using non-redundant aperture masking experiment at Palomar do not show this kind of morphology. One must notice that these maps concerned the photosphere and the molecular atmosphere of Mira, although the COME-ON+ maps of Figs. 6 to 8 concern the dust shell.

As for the Red Rectangle, we are tempted to interpret this small X shape as due to the light scattered by the dust material distributed at the surface of a bicone. The presence of a close companion star tends to make this hypothesis more convincing (Morris 1987). Further high angular observations at a lower level (with a higher dynamic range) are really needed to confirm the X shape of the shell and the presence of the elongated structures appearing in J, possibly aligned on the X.

5. Conclusions

The use of the COME-ON+ adaptive optics system has allowed us to resolve the dust shell of five late-type stars in the near infrared. These observations, all in agreement with previous high angular resolution ones, clearly show that aspherical dust shell is a common feature of the late stages of stellar evolution, as already concluded from polarization measurements (Johnson & Jones 1991).

The gap between the range of angular resolution from 0.1 ″ to 1 ″ allowed by infrared adaptive optics and the range below 0.1 ″ allowed by long baseline interferometry is now disappearing. This leads to a better understanding of both the post-AGB phase, where the dust shells are often extended and generally thick, and the AGB one, where a more tenuous shell is found to be closer to the star.

Acknowledgements. We are grateful to Drs. W.C. Danchi, C. Dougados, M. Faucherre, P. Ghez, J. Lefèvre, D. Mékarnia, G. Perrin, J.-L. Starck and Pr. C.H. Townes for their contribution in the definition and

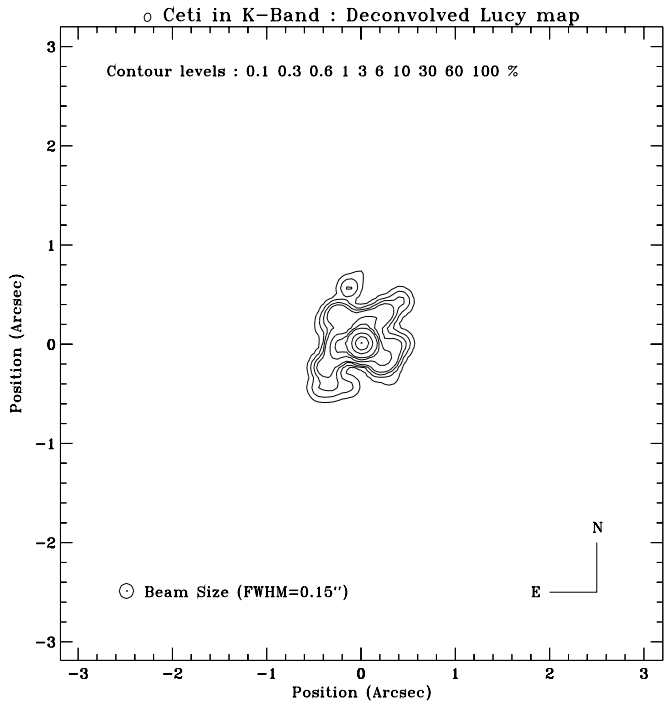

Fig. 8. Reconstructed Lucy map of o Ceti in K-band (600s of total integration time). North is up and east is left. The angular resolution is 0.15″. Overplotted contours are 0.1, 0.3, 0.6, 1, 3, 6, 10, 30, 60, and 100% of the maximum of intensity

the preparation of the mission. We also wish to thank the whole COME-ON+ team that made these observations possible, as well as the ESO La Silla and Garching staff for helpful assistance. The University of California portion of the work has been supported by a grant from the National Science Foundation (Grant N° AST-9315485).

References

Allen, D.A. et al., 1977, ApJ 217, 108, 113
Babcock, H.W. 1953, PASP 65,194
Bartelt, H. et al., 1984, Appl. Opt. 23, 3121
Bedding, T.R. et al., 1994, A&A 290, 340
Bensammar, S. et al., 1985, A&A, 149, L1
Bester, M. et al., 1996, ApJ 463, 336
Bloemhof, E.E. et al., 1984, ApJ 276, L21
Böker, T. et al., 1994, A&A 288, 656
Bonneau, D. et al., 1982, A&A 106, 235
Cohen, M. et al., 1975, ApJ 196, 179
Cruzalèbes, P. et al., 1996, A&ASS 116, 597
J.C. Dainty, J.C. et al., 1985, ApJ 293, 530
Danchi, W.C. et al., 1990, ApJ 359, L59
Danchi, W.C. et al., 1992, in High-Resolution Imaging by Interferometry II, J.M. Beckers and F. Merkle (eds.), Vol. 39, pp. 21-32, ESO
Danchi, W.C. et al., 1994, AJ 107, 1469
Dougados, C. 1991, University of Paris VII, France
Dyck, H.M. et al.,, 1984, ApJ 287, 801
Eckart, A. and Duhoux, Ph., 1990, in: Astrophysics with Infrared Arrays, R. Elston (ed.), Vol. 14, pp. 336, ASP Conf. Series
Haniff, C.A. et al., 1992, AJ 103, 1662
Herbig, G.H., 1970, Contrib. Lick Obs. 302, 13
Heske, A. et al., 1989, A&A 218, L5
Hofmann, R. et al., 1993, in: Progress in Telescopes and Intsrumentation Techniques, M.H. Ulrich (ed.), Vol. Report 42, pp. 617, ESO
Hyland, A.R. et al., 1969, ApJ 158, 619
Johnson, J.J. and Jones, T.J., 1991, Aj 101, 1735
Karovska, M. et al., 1991, ApJ 374, L51
Karovska, M. et al., 1993, ApJ 402, 311
Leinert, Ch. and Haas, M., 1989, A&A 221, 110
Lopez, B. et al., 1995, A&A 296, 752
Lopez, B., et al., 1997a, ApJ 488, 807
Lopez, B. et al., 1997b, A&A 322, 868
Lucy, B.J. et al., 1974, AJ 79, 745
Meixner, M., 1993, Ph.D. thesis, University of California at Berkeley, CA United States
Monnier, J. et al., 1998, in prep.
Morris, M., 1987, PASP 99, 1115
Quirrenbach, A. et al., 1992, A&A 259, L19
Quirrenbach, A. et al., 1994, A&A 285, 541
Richichi, A. and Lisi, F., 1990, A&A 230, 355
Richichi, A. et al., 1995, A&A 301, 439
Rigaut, F. et al. 1991, A&A 250, 280
Roddier, F. et al., 1995, ApJ 443, 249
Rouan, D., 1993 in: Mass Loss on the AGB and Beyond, Schwarz (ed.), ESO/CTIO Rowan-Robinson, M. and Harris, S., 1983a, MNRAS 202, 767
Rowan-Robinson, M., and Harris, S., 1983b, MNRAS 202, 797
Tessier, E. et al., 1990, in: Astrophysics with Infrared Arrays, R. Elston (ed.), Vol. 14, pp. 145, ASP Conf. Series
Tuthill, P.G., 1994 1994, University of Cambridge, UK
van der Hucht, K.A. et al., 1980, A&A 82, 14
Wilson, R.W. et al., 1992, MNRAS 257, 369